Effects of supersaturation on the structure and properties of poly(9,9-dioctyl fluorene) organogels

ARTICLE *in* SOFT MATTER · DECEMBER 2013

Impact Factor: 4.03 · DOI: 10.1039/c3sm51753e

3 AUTHORS, INCLUDING:

Pablo De la Iglesia
University of Washington Seattle
9 PUBLICATIONS **14** CITATIONS
SEE PROFILE

Lilo Pozzo
University of Washington Seattle
62 PUBLICATIONS **554** CITATIONS
SEE PROFILE

Soft Matter

RSC Publishing

PAPER

View Article Online
View Journal | View Issue

Cite this: *Soft Matter*, 2013, **9**, 11214

Effects of supersaturation on the structure and properties of poly(9,9-dioctyl fluorene) organogels†

Pablo de la Iglesia and Danilo C. Pozzo*

Rheological and small angle neutron scattering (SANS) measurements are used to characterize the gelation of poly(9,9-dioctyl fluorene) in organic solvents. The effect of supersaturation over the system's structure and properties is quantified. A variable range of solvent compositions and temperatures are used to control supersaturation. The mechanical and structural properties of the gels are characterized under different gelation conditions. Rheological studies reveal a strong dependency between the level of supersaturation of the system and the gelation kinetics. Samples start gelling faster and form stronger gels as the supersaturation of the system increased by lowering the temperature. Fits using the Avrami theory of phase change reveal a systematic variation in the dimensionality of the networks as the driving force for gelation is varied. A lower dimensionality is found for gels formed at lower supersaturation, whereas higher dimensionality typical of bifurcated networks appears as the supersaturation increases. SANS and USANS experiments also provide insight into structural variations occurring over several length scales. A power law dependence appears at low-q ($6.0 \times 10^{-4} < q < 4.0 \times 10^{-3}$ Å^{-1}) showing a higher exponent at low supersaturation indicating the formation of polymer-rich and solvent-rich domains with a well defined interface. Meanwhile, at higher supersaturation, the exponent value systematically decreases indicating that a more intermixed network–solvent system is formed. This is also corroborated with sTEM images for several polymer–solvent systems. The system's conductivity is also probed during gelation but there are no observable differences between the sol and the gel states for any of the systems. This study demonstrates the possibility of controlling network structures in conjugated polymers by changing the driving forces that are used for aggregation so that it may be possible to optimize the structure of organogels for specific applications.

Received 26th June 2013
Accepted 4th October 2013

DOI: 10.1039/c3sm51753e

www.rsc.org/softmatter

Introduction

Conjugated polymers (CPs) are versatile materials due to their unique optical and electronic properties and because they can be used for applications in photovoltaic devices, light-emitting diodes, transistors and organic sensors among many others.[1–4] Although uses for these materials are often limited by inefficient charge transport, it has been shown that crystallization of the polymer can sometimes result in more efficient charge propagation.[5,6] This is caused by an increase in overlapping of orbitals due to chain packing and ordering. Moreover, conjugated polymers tend to aggregate to form fibers, sheets and other organized multi-chain assemblies.[7–9] In concentrated solutions, such aggregates can also interconnect to form percolating organogels.[10–12] The formation of organogels is usually only possible in solvents of moderate solubility for the polymer. If the polymer is too soluble, the sample never aggregates to form gels. In contrast, if the polymer is too insoluble in a specific solvent, it remains permanently associated with other chains so that it cannot fully dissolve and, therefore, cannot gel. Consequently, the gelation of conjugated molecules is usually induced by gradually decreasing the solubility of a conjugated polymer in solvents of modest quality by systematically altering the solvent composition (*i.e.* adding a miscible non-solvent) or by changing the temperature.

Gel formation has been reported for a number of conjugated polymers, including poly(3-alkyl-thiophene) (P3ATs), poly(9,9-dialkyl fluorene) (PFAs) and poly(vinylene phenylene) (PVPs), showing that this is common behavior in these systems.[8,13,14] The aggregation of the polymer strands often modifies the absorbance and luminescence behavior of the system.[15–17] The changes observed in the photophysical properties are caused by differences in the conformation of the polymer chains in the dissolved and aggregated states. It has also been shown that the conductivity of P3HT films can increase by several orders of magnitude when polymer gels are formed.[9] The formation of fiber networks in P3HT can facilitate charge transport by two different mechanisms. First, a coil-to-rod transition causes a substantial increase in conjugation-length of the individual

Department of Chemical Engineering, University of Washington, Box 351750, Seattle, Washington 98195-1750, USA. E-mail: dpozzo@u.washington.edu

† Electronic supplementary information (ESI) available. See DOI: 10.1039/c3sm51753e

polymer strands and this improves intra-chain charge propagation. Secondly, the reduced distance between stacked polymer chains (*i.e.* due to pi–pi stacking) that form the fibers and nanostructures facilitates inter-chain charge hoping events that also increase charge conduction. However, despite these increases in conductivity, it has also been determined that controlling the structure and connectivity of the organogel networks is critically important to take full advantage of this approach to enhance electronic properties.[11,12]

The degree of aggregation and the structural characteristics of organogel networks (*e.g.* cross-sectional dimensions and fiber connectivity) formed from conjugated polymers are also strongly dependent on the specific conditions of the experimental systems (*e.g.* polymer backbone chemistry, solvent type, molecular weight, concentration and gelation temperature). Ultimately, all of these parameters can individually affect the driving force for aggregation (*i.e.* supersaturation) and therefore change the kinetics of gelation. Furthermore, it has also been shown that the kinetics of gelation is critically important for determining the final structure of these materials. In fact, the degree of supersaturation has been found to be one of the most important parameters in the description of the development of organogels formed out of small molecules.[18,19]

In this study we explore the gelation behavior of poly(9,9-dioctyl fluorene) (PFO) in various organic solvents using rheology and small angle neutron scattering (SANS). The gelation of PFO has been previously studied in solvents such as methylcyclohexane and toluene. Scattering and spectroscopy techniques were primarily used to study gelation kinetics in these systems.[7,13,15,20–22] In these studies, the small angle scattering of the PFO–solvent system transitions from a power-law dependence with an exponent of -1 for the fully dissolved polymer solutions to a -2 power-law exponent in the crystallized/gel state.[7] This change, hints to an evolution of the polymer conformation from stiff rod-like polymer chains to sheet-like structures.[7,22] The presence of the sheet polymer conformation is corroborated using UV-Vis absorption spectroscopy by the existence of a characteristic absorption peak at 437 nm.[15] It has been previously shown that these sheets facilitate the gelation of the PFO system.[21] However recent studies show that the abundance of this phase is small compared to the quantity of the overall polymer aggregates and the crystalline domains are trapped within amorphous macroscopic aggregates.[20] The present work studies the changes occurring in the mesoscopic structure of PFO gels as a function of variations in the solution conditions in which they are formed. The main focus of the study is to systematically explore the differences over rheological, and structural properties produced by controlling the driving force of aggregation. With this work we start laying the groundwork for efficiently engineering polymer gel systems to be used in specific applications.

Experimental methods

Materials

Poly(9,9-dioctyl fluorenyl-2,7-diyl) (PFO) is purchased from Sigma-Aldrich (St Louis, MO). The polymer has a molecular weight of 35 500 g mol^{-1} and a PDI of 2.6, as measured by GPC using polystyrene standards. The hydrogenated solvents, toluene, *o*-dichlorobenzene, dodecane, *m*-xylene, and mesitylene, are purchased from Sigma-Aldrich and are used as received. Fully deuterated solvents, used in neutron scattering experiments, are purchased from Cambridge Isotopes (Andover, MA) and are also used as received. The concentration of all solutions is kept at 30 mg of PFO per 1 ml of solvent. In order to fully dissolve the polymer in each solvent, the mixture is agitated and heated to 85 °C. In dodecane, it was necessary to heat the sample up to 100 °C due to the poor solvent quality.

Scanning transmission electron microscopy (sTEM)

A FEI (Hillsboro, OR) Tecnai G3 F20 transmission electron microscope (TEM) is used for scanning transmission electron microscopy (sTEM). The samples are prepared by adding 0.5 ml of the fully dissolved PFO mixtures into a capped glass vial for gel formation. To form the gels, samples containing *m*-xylene, toluene and mesitylene are left in the freezer at -20 °C overnight. Samples in *o*-dichlorobenzene are formed in a Peltier dry bath set to -15 °C overnight. Dodecane, which is a very poor solvent for PFO, is also allowed to form gels at 25 °C overnight. In order to mount samples on TEM grids, 2 ml of each solvent is added after gelation into corresponding vials and the sample is subsequently fractured by agitation. A drop of the fractured fluid dispersion is then deposited on an ultrathin, TEM copper grid with carbon support (Ted Pella, Redding, CA), and it is allowed to dry overnight before analysis.

Small amplitude oscillatory rheology

An Anton Paar (Ashland, VA) MCR 301 stress controlled rheometer is used with a parallel plate geometry of 25 mm in diameter and 0.4 mm gap between the plates. The gelation of the solutions is tracked while applying a sinusoidal strain of amplitude 0.1% at a constant frequency of 1 Hz. Under these conditions, all samples are well within the linear viscoelastic regime when the gel is fully formed [ESI†]. The temperature of the sample is accurately controlled with Peltier devices on both plates. The samples are loaded into the rheometer immediately after heating so that the polymer is in a fully dissolved fluid state. The rheometer plates are also pre-heated to a temperature that is high enough for the gel to not form instantaneously upon contact (*i.e.* 60 °C for dodecane samples and 25 °C for all other solvents). To prevent sample evaporation, an immiscible perfluorinated solvent Fomblin Y LVAC 25/6 from Sigma-Aldrich (St Louis, MO) is placed around the entire circumference of the plates sealing all of the exposed edges of the samples. The sample is then quickly quenched, using a rate of approximately 15 °C min^{-1}, to the desired final temperature (-20 °C for toluene, *m*-xylene, mesitylene; -15 °C for *o*-dichlorobenzene; and various temperatures for dodecane). For PFO dissolved in dodecane, the samples are heated to 100 °C for 1 minute immediately after loading, in order to ensure that they are fully dissolved before quenching and commencing the experiment.

Small angle neutron scattering (SANS)

Small angle neutron scattering (SANS) experiments are performed at the Center for Neutron Research at the National Institute of Standards and Technology (NIST) in Gaithersburg, Maryland. The SANS experiments are performed using both the NG3 and NG7 instruments. SANS is performed using a standard configuration to cover a wide range of wavevector values ($0.002 < q < 0.3$ Å^{-1}),[23] using wavelengths of 5.5, 6 and 8.09 Å. The data are reduced and corrected by accounting for background radiation and scattering from the sample cell. The data are also normalized to an absolute scale by measuring the incident neutron flux.[24] In addition, ultra-small angle neutron scattering (USANS) experiments are performed using the perfect crystal diffractometer BT5 at the NIST-NCNR.[25] This increases the total q range to 3×10^{-5} Å^{-1} so that micrometer sized features can also be probed. For each measurement, the samples are taken directly from the SANS instrument (NG3 or NG7) and placed into BT5 so that identical and fully equilibrated structures are probed. Samples for neutron scattering are prepared by loading the fully dissolved polymer (hot) into a demountable titanium cell. The solution is then heated again inside the cell in order to fully re-dissolve the sample. Mixtures of PFO in d-xylene, and d-toluene are allowed to gel overnight at −20 °C while the sample in *o*-dichlorobenzene is allowed to gel overnight at −15 °C to prevent freezing of the solvent. Five samples of PFO in d-dodecane are also allowed to gel overnight at 25, 32, 40, 50 and 60 °C. Gels formed in d-dodecane mixtures are exposed to the beam at the same temperatures in which they are formed. All other samples are run at 20 °C. All USANS measurements are performed at room temperature. Reduction of the data is performed using the standard NIST Igor-based macros.[24] Analysis and model fitting is also performed using the NIST Igor-based analysis software and the DANSE SansView software.[24] The models, fitted to the data, are modified to account for the different collimation of the systems using the tools available in the software packages. Corrections for incoherent scattering are also performed by assuming that, at the largest measurable scattering vectors ($q > 2$ Å^{-1}), the scattering intensity is dominated by a flat incoherent background signal.

Scattering model fitting

The model used to analyze the data on the high-q region (0.07 Å$^{-1} < q < 0.2$ Å^{-1}) is the Guinier–Porod model. This shape-independent form factor is used to analytically obtain the dimensionality and characteristic length scale of asymmetric objects that are characterized by a smooth transition from a Guinier region to a Porod region.[26]

The Guinier–Porod model uses the following form factors:

$$I(q)\begin{cases}\phi\Delta\rho^2 \exp\left[\dfrac{-q^2 {R_g}^2}{3-s}\right] & \text{for } q \le Q_1 \\ \dfrac{D}{q^m} & \text{for } q \ge Q_1\end{cases} \quad (1)$$

where ϕ is the volume fraction of the polymer, $\Delta\rho$ is the difference in scattering length density (solvent *vs.* domain), R_g is the radius of gyration of the system, s is a dimensionality parameter, and m is the slope at high q. D and Q_1 are defined as follows:

$$D = \phi\Delta\rho^2 \exp\left[\frac{-{Q_1}^2 {R_g}^2}{3-s}\right] {Q_1}^{(m-s)} \quad (2)$$

$$Q_1 = \frac{1}{R_g}\sqrt{\frac{(m-s)(3-s)}{2}} \quad (3)$$

by defining Q_1 as shown in eqn (3), the continuity of the Guinier and Porod functions and their slopes is enforced. The incoherent background is subtracted from the data before fitting with eqn (1).

The dimensionality parameter s is used to estimate the dimension of the primary scattering objects. The parameter s modifies the standard Guinier formula so that it is also possible to fit asymmetric objects such as rods and platelets.[27] When $s = 0$ the standard Guinier formula is recovered, indicating objects with a globular or 3-D structure. If $s = 1$ the model indicates the presence of rods, and $s = 2$ for lamellar structures. It is important to point out that this model is still valid for intermediate shapes between spheres and rods, and between rods and platelets.[24]

Results

Gelation

The solvents used in this study cover a wide range of solvent quality for PFO. Toluene, *m*-xylene, mesitylene, and *o*-dichlorobenzene are relatively good solvents and solutions need to be cooled to very low temperatures to induce gelation. In order to gel within the time frame of 24 hours, these samples need to cool down to at least −20 °C; otherwise the gels take several days to form. In contrast, samples dissolved in dodecane only require temperatures below 60 °C to form stiff gels. Our studies show that fast gelation is generally observed in simple alkane solutions at modest temperatures while a very slow gelation is observed in aromatic solvents where temperatures need to be substantially lower. The gelation kinetics of PFO dissolved in different aromatic solvents also varies significantly depending on the functional groups that are attached to the aromatic rings. Functional groups, such as chlorine (*o*-dichlorobenzene), nitrogen (pyridine) or sulfur (thiophene), result in gelation at higher temperatures and in shorter periods of time when compared to aromatics having simple alkane-functional groups (toluene, xylene, and mesitylene).

Fig. 1a shows a picture of a typical sample of PFO dissolved in *m*-xylene before and after gelation. Upon gelation, samples typically become cloudy and opaque due to increased light scattering indicating the formation of large structural features. Fig. 1b–f show sTEM images of PFO gels formed in toluene, *m*-xylene, mesitylene, dodecane and *o*-dichlorobenzene respectively, the gels are all prepared as indicated in the Methods section. These images clearly reveal different structures formed by the same polymer when it is gelled in different solvents. Samples gelled in toluene and mesitylene (Fig. 1b and d) appear

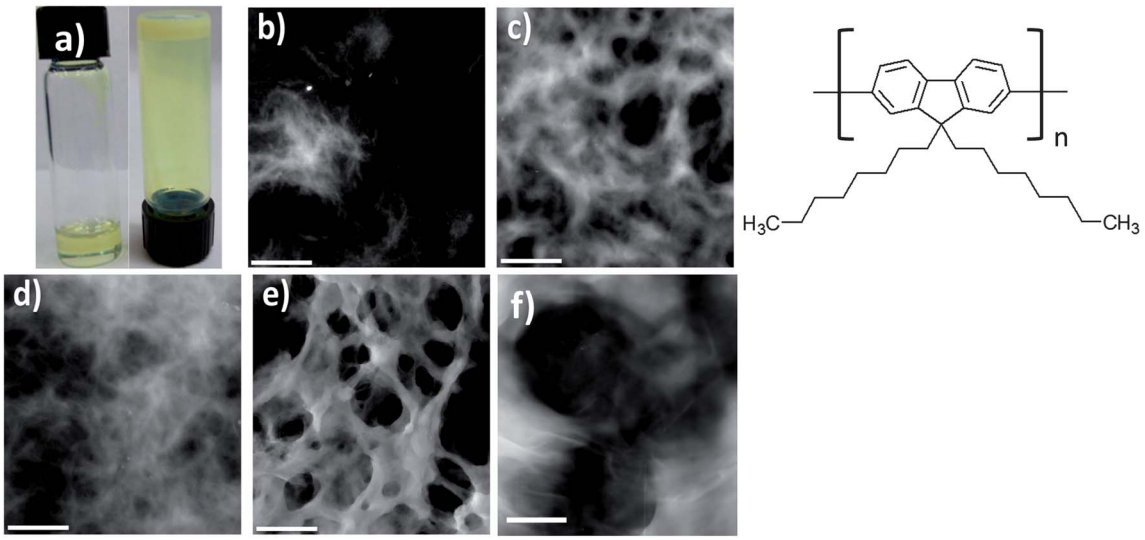

Fig. 1 (a) Photograph of a 30 mg ml^{-1} PFO, in *m*-xylene, system before and after gelation. sTEM images of PFO structures formed in (b) toluene, (c) *m*-xylene, (d) mesitylene, (e) dodecane, (f) *o*-dichlorobenzene. Scale bars represent 2 μm. All samples are gelled overnight and fractured in order to mount on the TEM grids. Additional sTEM images of all the systems can be found in the ESI.† The chemical structure of PFO is also shown.

to be formed from the agglomeration of very small fibers that frequently form larger spherulitic domains. The structures of gels formed in *m*-xylene (Fig. 1c) and dodecane (Fig. 1e) and *o*-dichlorobenzene (Fig. 1f) appear to be formed by sheets and, in these cases, larger pores are formed. Additional sTEM images are also provided in the ESI.†

Rheology

Fig. 2 shows the gelation kinetics of PFO in different solvents and the change in complex modulus (G^*) that is observed as a function of time (for frequency and strain sweeps of the system, that shows the samples gel behavior and their linear viscoelastic regime, please refer to Fig. S2 and S3 in the ESI†). The increase in complex modulus is caused by the aggregation of polymer chains to form interconnected nanoscale domains that can transduce stress throughout the sample. From these data, it is clear that *o*-dichlorobenzene is the worst aromatic solvent for PFO because gelation occurs the fastest, within one hour from the beginning of the run, even though it is held at a higher temperature (−15 °C) than the other aromatic solvents (−20 °C). Toluene appears to be the next poorest solvent followed by mesitylene, which has a gelation time that is similar to *m*-xylene. However, as gelation progresses, the complex modulus of the mesitylene sample increases above that of *m*-xylene and it eventually matches the complex modulus of the sample formed in toluene. Gels can be stronger either

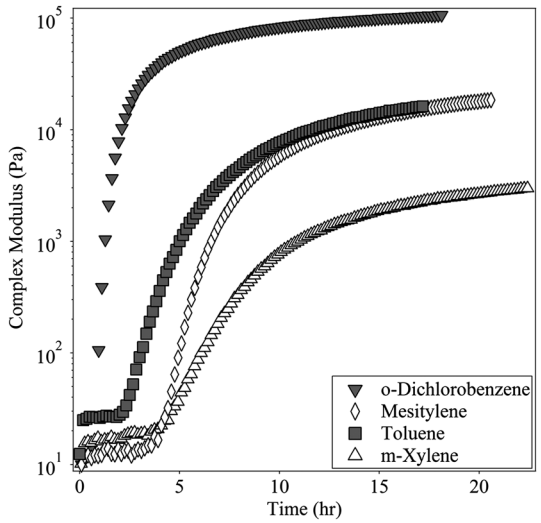

Fig. 2 Comparison of gelation kinetics of PFO in different aromatic solvents. The temperature is held constant in each run at −20 °C for the gel formed in *m*-xylene, mesitylene and toluene and at −15 °C for *o*-dichlorobenzene.

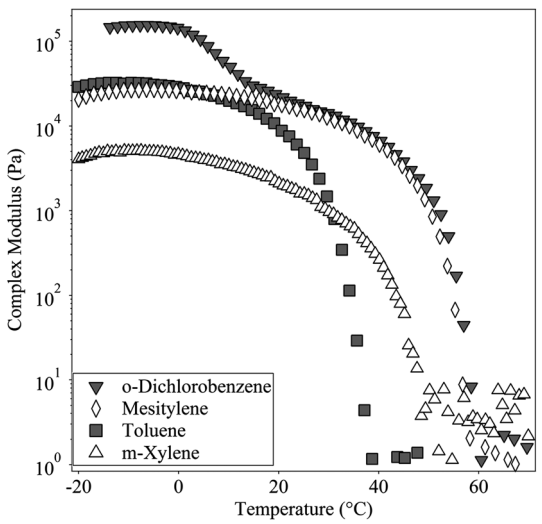

Fig. 3 Dissolution curves for PFO gels formed in different solvents at −20 °C for mesitylene, toluene and *m*-xylene and −15 °C for *o*-dichlorobenzene. The heating rate is 1 °C min^{-1}.

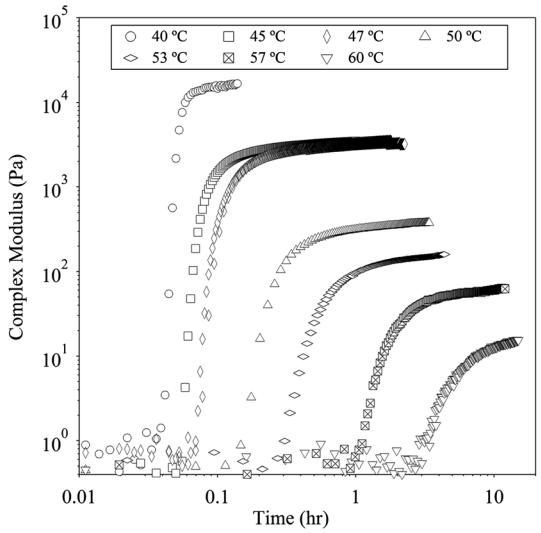

Fig. 4 Complex modulus (G^*) of PFO samples formed in dodecane, gelled isothermally at different temperatures.

because a larger percentage of polymer chains aggregate to form fibers in the network, or because stronger connections are formed between these domains.

Fig. 3 shows gel dissolution curves (heating) for the PFO organogel samples that are formed in different aromatic solvents. The heating data also suggest that *o*-dichlorobenzene is the worst solvent because it requires temperatures in excess of 60 °C for the gel to fully dissolve. Samples formed in mesitylene also require high temperatures to fully dissolve the polymer. In contrast, samples formed in *m*-xylene only require approximately 50 °C to fully dissolve. PFO organogels formed in toluene show smaller hysteresis, since they are among the fastest forming gels and dissolve at the lowest temperature (T_{dis} ~ 40 °C). When all of these samples are heated from their low gelation temperature to room temperature (~25 °C), the gels retain a significant amount of elasticity suggesting that the network structures are largely maintained. In the case of *o*-dichlorobenzene, there is an evident two-step decay of the complex modulus that does not appear in any of the other solvents. This observation is fully reproducible but, at this time, we are unable to fully explain the nature of the first transition step. It is presumed that the second step is related to the same dissolution process that PFO gels undergo in the other solvents.

Using a similar approach, the gelation of PFO at different temperatures is also analyzed using small amplitude oscillatory rheology. We take advantage of the poor solvent quality of dodecane to induce gelation of PFO over a range of temperatures (40 to 60 °C) in order to probe the evolution of the gel structure at different levels of supersaturation. Fig. 4 shows the gelation runs of PFO in dodecane. At low temperatures, the onset of gel formation occurs over a few minutes due to the high driving force for inducing gelation (*i.e.* high supersaturation of the system). As the temperature increases, the onset time systematically decreases to the range of several hours due to the lowering of the degree of supersaturation. The behavior of the complex modulus of the systems is also similar when probing at much lower perturbation frequencies (0.01 Hz), indicating that the gelation of the system is independent of the perturbation frequency of the measurement (see Fig. S4 in the ESI†). The temperature that is used to drive the aggregation also affects the final elasticity of the gels (G^*) after gelation is complete. Weaker gels are formed at higher temperatures or lower levels of supersaturation. Similar behavior is also observed

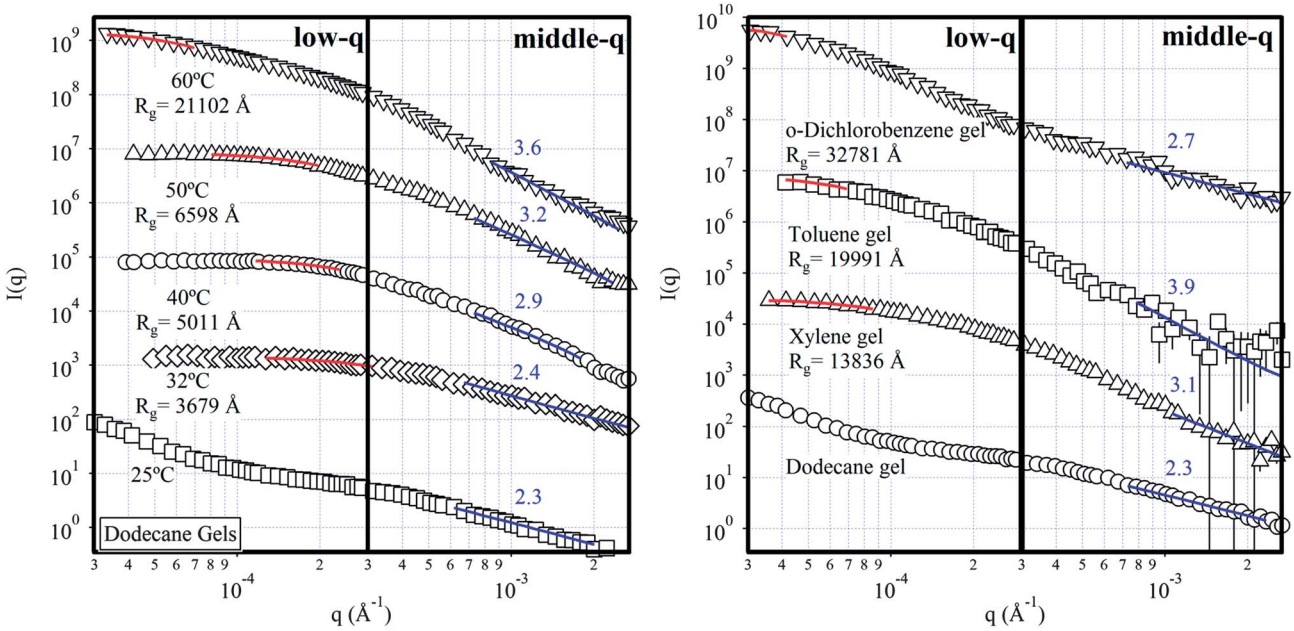

Fig. 5 Left: USANS profiles (smeared) of the PFO gels formed at different temperatures in d-dodecane. Right: USANS profiles corresponding to the samples formed in different solvents; d-toluene (−20 °C), d-xylene (−20 °C), *o*-dichlorobenzene (−15 °C) and d-dodecane (25 °C). The solid lines correspond to fits to the Guinier equation and the values of R_g are also provided. Curves are shifted vertically for adding clarity.

Table 1 Parameters obtained from the fits to the neutron scattering data

	o-Dichlorobenzene	Toluene	*m*-Xylene
R_g from Guinier–Porod model (nm)	2.7 ± 0.1	1.9 ± 0.1	2.1 ± 0.1
High-q power law exponent [m]	3.8	2.3	3.8
Dimensional parameter [s][28]	1.5	1.4	1.7
Low-q power law exponent	2.7	3.9	3.1
Network R_g (nm)	3278 ± 132	1999 ± 101	1383 ± 34

Dodecane					
Temperature	25 °C	32 °C	40 °C	50 °C	60 °C
R_g from Guinier–Porod model (nm)	3.1 ± 0.1	3.0 ± 0.1	2.2 ± 0.1	2.6 ± 0.1	3.3 ± 0.1
High-q power law exponent [m]	3.1	3.0	3.0	2.9	3.0
Dimensional parameter [s]	2.0	2.0	1.9	1.9	1.9
Low-q power law exponent	2.3	2.4	2.9	3.2	3.6
Network R_g (nm)	N/A	367 ± 19	501 ± 10	659 ± 8	2110 ± 16

with samples formed in different solvents (Fig. 2). In general, the systems that gel faster are also the ones forming the stronger gels.

Small angle neutron scattering

Fig. 5 shows the USANS scattering profile for the PFO gels formed in different solvents and at different temperatures. At low q, the scattering experiment probes the larger features of the network structure. In this q-range, a Guinier plateau region appears for all the gels indicating that a characteristic structural feature of micrometer size is present in all samples. However, the sample of PFO that is gelled in dodecane at room temperature also shows a second uptake after the Guinier region that does not appear in any other sample. A fit to the Guinier equation (eqn (4)) is applied to all samples over this portion of the profiles.[28]

$$I(q) = \phi\Delta\rho^2 \exp\left[\frac{-q^2 R_g{}^2}{3}\right] \quad (4)$$

The radius of gyration (R_g) characterizing the largest features of the PFO networks is obtained from this analysis and the results are included in Table 1 for the different solvent samples. A trend of increasing feature size is observed for the aggregates formed at higher supersaturation (*i.e.* decreased R_g as gelation temperature decreases).

Power-law dependencies (*i.e.* linear region in log–log plot) also appear in the q-range corresponding to 6.0×10^{-4} to 4.0×10^{-3} Å^{-1} (middle-q region) for all PFO gel samples with

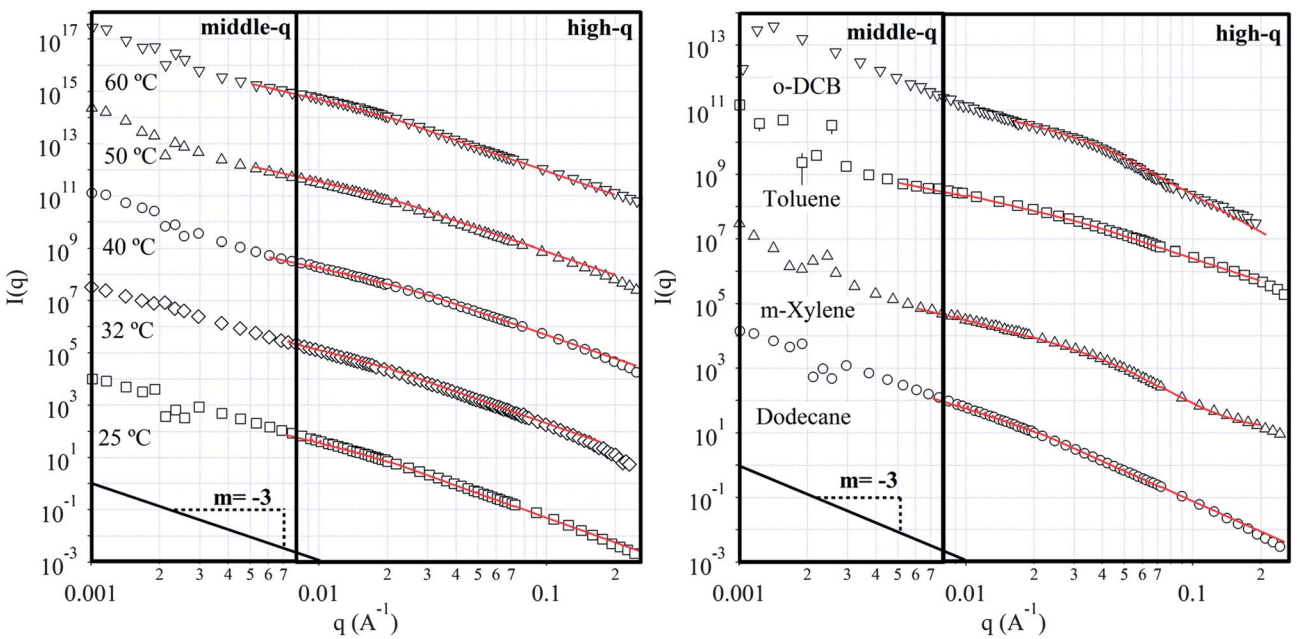

Fig. 6 Left: SANS scattering profiles of the gels formed at different temperatures in d-dodecane. Right: profiles corresponding to the samples formed in different solvents. The solid, red lines are fits obtained from the Guinier–Porod model. The parameters obtained from these fits are listed in Table 1.

exponents ranging in value from −2.3 to −3.6 (Fig. 5 and 6). These values are characteristic of sharp interfaces being formed in the samples between regions with clearly different values of scattering length density. This suggests that the networks (polymer-rich regions) can be well segregated from polymer–poor solvent regions between them (*i.e.* a heterogeneous polymer distribution) and that this segregation varies with solvent and conditions used for gelation.[29] There is a clear trend of decreasing power-law exponent as the supersaturation of the system increases. For example, there are higher power-law exponents when the temperatures increase in dodecane gels and the exponents of the PFO gels formed in *o*-dichlorobenzene are also smaller than those of gels formed in *m*-xylene. All power-law exponent values are also listed in Table 1.

Over the SANS q-range of 4×10^{-3} and 5×10^{-2} Å^{-1} (high-q), the formation of a characteristic 'knee' is evident in all the gel samples (Fig. 6). This 'knee' is also observed in P3HT organogel samples and it can be related to the cross-sectional geometry of the building blocks of the networks (*e.g.* nanofibers or nanosheets). The q dependence of the scattering in this region generally fluctuates from power-law exponents of −3 to −2. At the lower end, this can be characteristic of the organization of PFO polymer chains into sheet-like two-dimensional structures.[7,22] However, fractal network structures are also known to give power-law exponents in this range. Finally, at high-q the scattering intensity rapidly decreases toward zero after the incoherent background is subtracted as discussed in the Experimental section.

Discussion

Controlling the driving force for aggregation of PFO strands is achieved by using different solvents or by allowing gel formation to occur at different temperatures. The sTEM images (Fig. 1) show marked differences in the morphology of the resulting samples. The neutron scattering results (Table 1) also validate the differences of the micron-scale morphology for gels formed with different gelling conditions. The samples also present different rheological behavior at different supersaturation levels. The gels formed at a high level of supersaturation have a higher modulus than the ones formed at lower levels. This may be due to more polymer chains going from the dissolved state to the aggregated state or to a change in the morphology of the networked domains. The fraction of dissolved polymer that remains after gelation is also measured by adding solvent to a gelled sample, physically breaking the gel, centrifuging the solids out and performing spectroscopic analysis of the remaining dissolved material. UV-Vis absorbance is used to estimate how much polymer remained dissolved after gelation under different conditions. We find that virtually all the polymers are aggregated in all samples independently of the conditions at which the gel is formed. Therefore, the differences in rheological properties are most likely due to the different conformation of the polymers in the networked structures and not to differences in the number of chains that are gelled.

In order to better quantify the effect of supersaturation on the kinetics of gel formation, a model derived by Liu and coworkers using Avrami theory of phase change is applied to the rheological data of different PFO organogel systems.[30]

$$X_{cr}(t) = \frac{G(t) - G_0}{G_f - G_0} \quad (5)$$

Eqn (5) relates the extent of aggregation X_{cr} (*i.e.* how far has gelation progressed from the initial dissolved state) using the temporal evolution of the complex modulus $G(t)$. G_0, and G_f correspond to the initial and final complex modulus respectively. The value of G_f is assumed to be the complex modulus when it has stopped from evolving in any meaningful way, at this point the sample is assumed to be fully developed. This method has been previously used to quantify the effect of solvent quality on the self-assembly of P3HT organogels.[11]

By monitoring the isothermal change over time, we obtain parameters describing the kinetics of network growth using eqn (6), where t_g is the onset time of gelation, k^0 is the rate growth constant and D_f is the fractal dimension of the system.

$$\ln[1 - X_{cr}(t)] = -k^0(t - t_g)^{D_f} \quad (6)$$

From the rheology, the parameters t_g, G_0, G_f are known and, by using these values to constrain the fit, it is possible to obtain a value for the fractal dimension (D_f). A D_f of 1 indicates that the networks are growing at a characteristic rate corresponding to one-dimensional aggregates (*i.e.* straight fibers). Values ranging between 1 and 2 indicate bifurcated or branching fiber growth, between 2 and 3 indicates spherulitic or sheet-like structures, and a D_f value of 3 indicates that the system is growing at an equivalent rate in all directions (*i.e.* 3-dimensional growth).

Fig. 7 shows the fits to the kinetic model using the rheological data. The parameters obtained from the fits indicate that the system with the highest fractal dimension is *o*-dichlorobenzene gel (2.49), followed by mesitylene and toluene PFO samples (2.18 and 2.19), and finally the gel formed in *m*-xylene (1.89). These results show an inverse correlation of this fractal dimension with solvent quality. It is important to point out that these fractal dimensions are also more correlated with the maximum storage modulus of the system than to the onset time for gelation (Fig. 2). The same trend can also be observed for the variable temperature experiments. As dodecane becomes a better solvent for PFO (*i.e.* by raising the temperature), the fractal dimension obtained from rheology steadily decreases (Fig. 7). For the fits performed to the rheological data of the temperature series, please refer to Fig. S4 in the ESI.†

The nanostructure of the gel is also affected by the extent of supersaturation. Previous work has shown a drastic change in network structures formed by P3HT in different solvents.[16] The sTEM images also reveal important structural differences of PFO aggregates in different solvents. There is also general consistency between the sTEM images (Fig. 1) and the rheological behavior of the samples (Fig. 2). Dodecane samples, at room temperature, appear to be the strongest of the gels, and on the sTEM images they appear to be formed out of thicker networked domains. The complex modulus of all dodecane samples are reported at temperatures that are way above room temperature and, despite this, they are still comparable with the

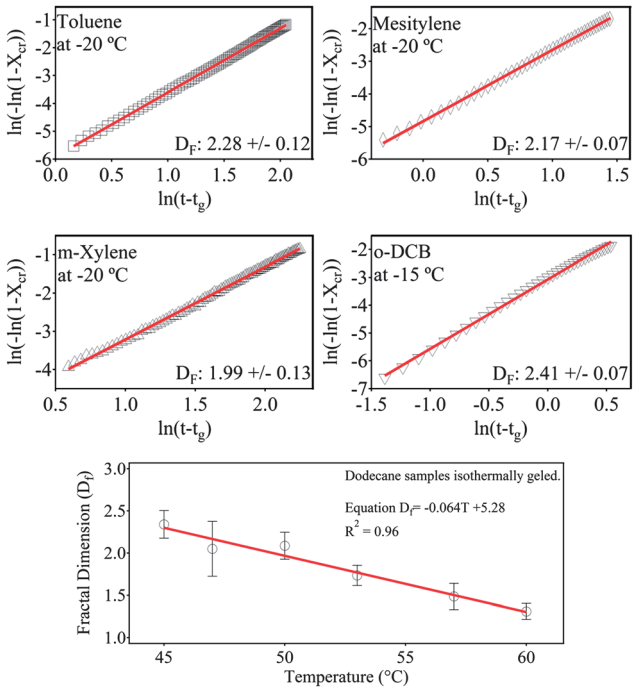

Fig. 7 Top graphs: representative Avrami curves for each of the aromatic solvent systems. The solid red lines are the fits obtained using Liu's model for gelation. Bottom graph: fractal dimension as a function of temperature for dodecane gels. The fractal dimension was obtained by fitting Liu's model to the data (ESI†).

modulus of the gel samples formed in other solvents. Gels formed in mesitylene and toluene appear to be composed of similar structures, and they both present a comparable complex modulus. In contrast, the structure of PFO gels formed in *m*-xylene does not resemble any of the other samples, even though the complex modulus has similar values (Fig. 1 and 2). Furthermore, out of all the aromatic solvents, gels formed from *o*-dichlorobenzene are stronger and result in more dense sheet-like structures. Since sTEM requires removal of solvent and it cannot characterize the smallest features of the gels, we use SANS and USANS to explore variations in the structure of the gels without altering their natural state.

In order to obtain the scattering profile of the structure of fully developed gels, the samples are maintained at their respective gelation temperatures (*o*-dichlorobenzene −15 °C, toluene and *m*-xylene −20 °C, dodecane at various temperatures) for at least 12 hours. This amount of time ensures that the gel is close to be fully developed as indicated by Fig. 2 and 4, since the complex modulus of any the systems does not increase much more after that amount of time has passed. The Guinier region in the USANS regime (Fig. 5) reveals structures formed at micron-sized length scales. Based on the similar length scales, these are also the larger features (*i.e.* phase separation) that are observed in the sTEM images. In the temperature study (Fig. 5 left), there is a clear trend of the Guinier plateau to shift to lower q as the temperature is raised. This means that there are larger features formed when the supersaturation of the system decreases. This can be explained by the decrease in number of growing nucleation centers due to the lower driving force for aggregation. The decreased growth rate also leaves more polymer chains available to increase the size of the few growing network domains. At lower temperatures (higher supersaturation), many more nucleation centers grow in parallel and trap more polymer chains leading to the formation of denser but also smaller domains. In samples formed in different solvents (Fig. 5 right) the opposite trend appears to occur. When the supersaturation of the sample is lower, based on gelation time (rheology), smaller network domains are created. This suggests that specific solvent–polymer interactions may also be present and could greatly influence the structure of the resulting organogels.

The Guinier region at low q is followed by a power-law region for all the samples (Fig. 5 and 6, $\sim 3 \times 10^{-4} < q < 4 \times 10^{-3}$ Å^{-1}). The magnitude of the power-law exponent in this region (*i.e.* the slope in the log–log plot) is found to be inversely proportional to the supersaturation level of the system for both the temperature and the solvent studies. A higher slope (closer to −4) indicates that a clear network–solvent interface is present in the samples. This is possibly explained by considering the aggregation of 2D sheet-like domains. At high supersaturation this process is very chaotic and fast, causing a more disordered stacking of the polymer domains (bottom panels in Fig. 8). In contrast, at low supersaturation the aggregation process is slower allowing the polymer to stack more effectively and to grow into longer networked domains (top panels in Fig. 8).

At high q, the scattering describes the shape of the smallest building blocks in the network. In order to quantify the effect of supersaturation on PFO organogels, a form factor model is used to fit the scattering profiles in this region. We also note that form factors of different shapes (*i.e.* lamellar, parallelepiped, flexible elliptical cylinder) did not accurately describe the scattering profiles for any of the gels. The sTEM images also do not provide adequate insight into the shape of the smallest building blocks because of the lack of sufficient resolution to adequately probe the polymer conformation at these length scales. For

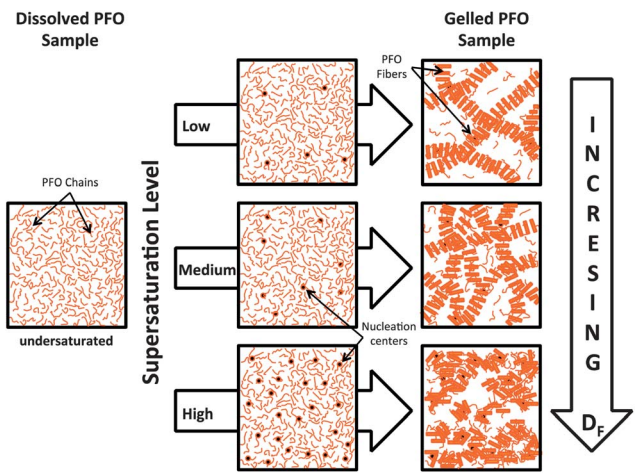

Fig. 8 Schematic description of the network conformations at different supersaturation levels. At low supersaturation (top) there are fewer nucleation centers formed. At high supersaturation (bottom) there is a high density of nucleation centers and fast growth causing the polymer to disorderly aggregate.

these reasons, a shape-independent form factor is used to fit the scattering profiles of the different organogel samples. The Guinier–Porod model is chosen for this purpose.[24] This way it is possible to quantify and compare the difference of the shape of polymer aggregates formed under different gelation conditions.

Fig. 6 shows the scattering data for all 8 samples with their corresponding fits. The parameters obtained from these fits are also listed in Table 1. It is obvious from the results that neither solvent nor temperature significantly affects the radius of gyration of the smallest building blocks in any meaningful way. This parameter stays constant between 2 and 3 nm for all the samples, even when a wide range of supersaturation is used. The constant value for this parameter is also consistent with a characteristic length that is likely controlled by the molecular properties of the polymer such as the contour length or the characteristic thickness of polymer strands that are stacked together. Similar observations are also made on a P3HT system, where the width and thickness of the fiber does not change with the solvent choice or solid concentration.[11] This suggests that the shapes and sizes of the organogel building blocks heavily depend on the polymer molecular characteristics.

The dimensionality parameter (s) approaches 2 for most of the samples. As explained previously, a dimensionality of 2 indicates the presence of sheet-like or lamellar structures. This is consistent with previous SANS studies performed on the PFO system.[7,22] However, as the supersaturation of the system is lowered in the solvent study, this dimensionality parameter also shifts towards lower values. Values between 1 and 2 indicate intermediate shapes between platelets and stiff cylinders. The change in dimensionality is due to the ordered aggregation that is caused by a decrease in supersaturation. The lack of a similar shift in the temperature study once more suggests that this change is likely due to the specific influence of the solvent on the polymer.

The high-q slope (Fig. 6, $0.04 < q < 0.15$ Å^{-1}) seems to be also affected by solvent choice. The value of this slope varies widely with solvent, but it again stays constant in the temperature study suggesting that it is related to specific interactions of the polymer with the solvents and not just to gelation kinetics. The slope in this region of q describes the molecular-scale polymer–solvent interface. A slope of -4 indicates a clear, discrete, and smooth interface between a solvent and the polymer domains (Porod behavior). The deviation from the -4 slope could indicate entrapment of solvent molecules within the polymer aggregates, which increases surface roughness and causes fluctuation in scattering length density at the interface. This entrapment is likely influenced by specific solvent–polymer interactions, and therefore would vary as a function of the solvent, but not as a function of the system's supersaturation. Nevertheless, it is important to point out that there is uncertainty in some of these values because the fits do not follow this portion of the data very closely for all of the samples and the incoherent scattering obscures the data at very high q (>0.15 Å^{-1}).

The self-assembly of PFO chains in organic solvents is clearly driven by the supersaturation of the system. This is probed by changing both the solvent type and/or the temperature that is used to drive isothermal gelation. The effect of varying the solvent type is highly complex because it can involve specific physical and chemical interactions between the polymer and the solvent molecules that are difficult to characterize at the length scales probed with these experiments. On the other hand, the temperature study keeps these molecular interactions constant, affecting only the aggregation kinetics. When there is only one factor controlling the extent of supersaturation (*i.e.* temperature variation study), there is a clear trend linking the onset time of gelation t_g to the maximum complex modulus G^* (Fig. 4). When the gels start forming earlier, the maximum complex modulus is higher. However, when there is not a complete control over all the factors driving aggregation, such as in the case of the solvent study, these trends do not always hold. For example, the gelation of PFO in mesitylene (Fig. 2) is considerably delayed when compared to the same sample in toluene even though its complex modulus eventually increases to a similar value. Also, the dissolution curves (Fig. 3) do not show the same solvent quality trend as the gelation curves (Fig. 2). Finally, the radius of gyration obtained from the USANS data (Fig. 5) also does not show the same trends for the solvent experiments as it does for the temperature study. This is again likely caused by the differences in the molecular interactions that develop between the different solvents and the PFO chains in each case.

Fig. 8 illustrates the general differences found for aggregation as the supersaturation of the system changes. Several nucleation centers are created in the samples when supersaturation is high (*e.g.* low temperature or bad solvent). The presence of many nucleation centers that grow simultaneously and very fast inhibits the growth of well-connected network domains. The result is a high fractal dimension and a heterogeneous sample. On the other hand, low supersaturation (*e.g.* high temperature or good solvents) inhibits the formation of nucleation centers in the sample. This leaves more polymer chains available for growth leading to a more organized and interconnected network. Low supersaturation makes aggregation less chaotic, minimizing defects that lead to the development of bifurcations or branches in the structure. Therefore, for these samples the fractal dimension of the system approaches 1-D growth. Using these extremes as a reference, it is possible to deduce a degree of supersaturation that will promote the growth of domains (*i.e.* prevent the simultaneous formation of a large number of nucleation centers), but at the same time facilitate interconnection of domains to create pathways for charge transport.

The different PFO–solvent systems are characterized by the schematic description shown in Fig. 8. At high supersaturation (*i.e.* higher driving force of gel formation), the shift of the Guinier plateau to higher-q (Fig. 5) indicates the presence of smaller subdomains. As the supersaturation of the system decreases (*i.e.* lowering the driving force of aggregation) the power law exponent at low-q systematically approaches -4 and the formation of larger subdomains is evident in R_g. The rheological analysis also supports this picture of the system, by showing a trend of increasing fractal dimension as the system's supersaturation increased (Fig. 7). Low fractal dimension and

larger domains are expected for ordered 1-D growth while high fractal dimension and small domains are expected for fast and chaotic growth.

When the conductivity of the sol and gel systems is measured, it turned out to be lower than the resolution of the instrument (Agilent E4980A Santa Clara, CA). Furthermore, upon gelation, the conductivity of the gels did not show an increase above the instrumental noise level (data in the ESI†). This is in direct contrast to findings in other studies involving different conjugated polymers.[11,12] This may be due to the differences in the intrinsic conductivity of the polymers or differences in the type of crystallization. WAXS data of a dry PFO gel show several crystal peaks characteristic with the α phase of PFO.[17] At the same time, the solid fraction of the PFO gels in all solvents is found to be very high so that the lower conductivity is not caused by a low fraction of PFO in the network phase.[20] This shows that aggregation and gelation of conjugated polymers does not necessarily cause a large increase in electrical conductivity. In contrast, P3HT organogels are formed from interconnected and highly crystalline nanowires (WAXS also in the ESI†) leading to a drastic increase in conductivity.[16] Fig. 3 shows a decrease in the complex modulus of fully formed gels when the temperature is raised. This implies that the gel structure fractures or breaks into smaller domains before the polymer chains fully disassociate from each other and the sample re-dissolves.

Conclusions

The gelation of a PFO system is characterized over different degrees of supersaturation and structural and rheological properties are quantified. In order to vary supersaturation, different solvents and temperatures are used to induce gelation of the polymer. It is found that supersaturation directly affects the gelation kinetics of the system and the overall morphology and structure of the networks. This study reveals a strong dependency of the rheological properties of the samples with the gelation conditions. sTEM and neutron scattering experiments show significant differences in the structure of the larger (micron-size) network features when gels are formed in different solvents and at different temperatures. The rheological fractal dimension is clearly affected by the level of supersaturation of the system further indicating a change in the network structure. In contrast, supersaturation plays a minor role in the structure of the smallest building blocks of the networks. This is analogous to the behavior of other conjugated polymer gels (*e.g.* P3HT) where molecular parameters control these features. In PFO, gelation does not appear to significantly increase the conductivity of the sample. This is again contrasting to other conjugated polymer systems (*e.g.* P3HT).

Acknowledgements

This work is primarily supported by the Department of Energy Office of Basic Energy Sciences under award number DE-SC0005153. We acknowledge the support of the National Institute of Standards and Technology in providing the neutron research facilities used in this work. This work utilized facilities supported in part by the National Science Foundation under Agreement no. DMR-0944772. This work benefitted from DANSE software developed under NSF award DMR-0520547 and from the use of the SWAXS instrument funded under the DMR-0817622 award. Part of this work was conducted at the University of Washington NanoTech User Facility, a member of the NSF National Nanotechnology Infrastructure Network (NNIN).

References

1 S. Guenes, H. Neugebauer and N. S. Sariciftci, *Chem. Rev.*, 2007, **107**, 1324–1338.
2 M. T. Bernius, M. Inbasekaran, J. O'Brien and W. S. Wu, *Adv. Mater.*, 2000, **12**, 1737–1750.
3 G. Horowitz, *Adv. Mater.*, 1998, **10**, 365–377.
4 V. C. Goncalves and D. T. Balogh, *Sens. Actuators, B*, 2009, **142**, 55–60.
5 H. Sirringhaus, P. J. Brown, R. H. Friend, M. M. Nielsen, K. Bechgaard, B. M. W. Langeveld-Voss, A. J. H. Spiering, R. A. J. Janssen, E. W. Meijer, P. Herwig and D. M. de Leeuw, *Nature*, 1999, **401**, 685–688.
6 J. F. Chang, B. Q. Sun, D. W. Breiby, M. M. Nielsen, T. I. Solling, M. Giles, I. McCulloch and H. Sirringhaus, *Chem. Mater.*, 2004, **16**, 4772–4776.
7 M. Knaapila, V. M. Garamus, F. B. Dias, L. Almasy, F. Galbrecht, A. Charas, J. Morgado, H. D. Burrows, U. Scherf and A. P. Monkman, *Macromolecules*, 2006, **39**, 6505–6512.
8 S. Samitsu, T. Shimomura and K. Ito, *Thin Solid Films*, 2008, **516**, 2478–2486.
9 S. Malik, T. Jana and A. K. Nandi, *Macromolecules*, 2001, **34**, 275–282.
10 L. L. G. Justino, M. Luisa Ramos, M. Knaapila, A. T. Marques, C. J. Kudla, U. Scherf, L. Almasy, R. Schweins, H. D. Burrows and A. P. Monkman, *Macromolecules*, 2011, **44**, 334–343.
11 G. M. Newbloom, K. M. Weigandt and D. C. Pozzo, *Macromolecules*, 2012, **45**, 3452–3462.
12 G. M. Newbloom, K. M. Weigandt and D. C. Pozzo, *Soft Matter*, 2012, **8**, 8854–8864.
13 C. Y. Chen, C. S. Chang, S. W. Huang, J. H. Chen, H. L. Chen, C. L. Su and S. A. Chen, *Macromolecules*, 2010, **43**, 4346–4354.
14 S. Malik and A. K. Nandi, *J. Polym. Sci., Part B: Polym. Phys.*, 2002, **40**, 2073–2085.
15 J.-H. Chen, C.-S. Chang, Y.-X. Chang, C.-Y. Chen, H.-L. Chen and S.-A. Chen, *Macromolecules*, 2009, **42**, 1306–1314.
16 G. M. Newbloom, F. S. Kim, S. A. Jenekhe and D. C. Pozzo, *Macromolecules*, 2012, **44**, 3801–3809.
17 S. H. Chen, H. L. Chou, A. C. Su and S. A. Chen, *Macromolecules*, 2004, **37**, 6833–6838.
18 J. L. Li, X. Y. Liu, R. Y. Wang and J. Y. Xiong, *J. Phys. Chem. B*, 2005, **109**, 24231–24235.
19 J.-L. Li, B. Yuan, X.-Y. Liu and H.-Y. Xu, *Cryst. Growth Des.*, 2010, **10**, 2699–2706.
20 L. Huang, X. Huang, G. Sun, C. Gu, D. Lu and Y. Ma, *J. Phys. Chem. C*, 2012, **116**, 7993–7999.

21 M. Knaapila, D. W. Bright, R. Stepanyan, M. Torkkeli, L. Almasy, R. Schweins, U. Vainio, E. Preis, F. Galbrecht, U. Scherf and A. P. Monkman, *Phys. Rev. E: Stat., Nonlinear, Soft Matter Phys.*, 2011, **83**, 051803.
22 M. Knaapila, R. Stepanyan, M. Torkkeli, V. M. Garamus, F. Galbrecht, B. S. Nehls, E. Preis, U. Scherf and A. P. Monkman, *Phys. Rev. E: Stat., Nonlinear, Soft Matter Phys.*, 2008, **77**, 051803.
23 C. J. Glinka, J. G. Barker, B. Hammouda, S. Krueger, J. J. Moyer and W. J. Orts, *J. Appl. Crystallogr.*, 1998, **31**, 430–445.
24 S. R. Kline, *J. Appl. Crystallogr.*, 2006, **39**, 895–900.
25 J. G. Barker, C. J. Glinka, J. J. Moyer, M. H. Kim, A. R. Drews and M. Agamalian, *J. Appl. Crystallogr.*, 2005, **38**, 1004–1011.
26 P. Lindner and T. Zemb, *Neutrons, X-rays and Light: Scattering Methods Applied to Soft Condensed Matter*, North Holland, Amsterdam, 2002.
27 O. Glatter and O. Kratky, *Small Angle X-Ray Scattering*, Academic Press, New York, 1982.
28 A. Guinier and G. Fournet, *Small-Angle Scattering of X-Rays*, John Wiley and Sons, New York, 1955.
29 A. M. Hecht, R. Duplessix and E. Geissler, *Macromolecules*, 1985, **18**, 2167–2173.
30 J.-L. Li and X.-Y. Liu, *Adv. Funct. Mater.*, 2010, **20**, 3196–3216.

